Systemic Delivery of Anti-miRNA for Suppression of Triple Negative Breast Cancer Utilizing RNA Nanotechnology

Dan Shu,[*,†,‡,§] Hui Li,[†,‡,§] Yi Shu,[†,‡,§] Gaofeng Xiong,[‡,∥] William E. Carson III,[⊥] Farzin Haque,[†,‡,§] Ren Xu,[‡,∥] and Peixuan Guo[*,†,‡,§]

[†]Nanobiotechnology Center, [‡]Markey Cancer Center, [§]Department of Pharmaceutical Sciences, [∥]Department of Pharmacology and Nutritional Sciences, University of Kentucky, Lexington, Kentucky 40536, United States and [⊥]OSU Comprehensive Cancer Center, The Ohio State University, Columbus, Ohio 43210, United States

ABSTRACT MicroRNAs play important roles in regulating the gene expression and life cycle of cancer cells. In particular, miR-21, an oncogenic miRNA is a major player involved in tumor initiation, progression, invasion and metastasis in several cancers, including triple negative breast cancer (TNBC). However, delivery of therapeutic miRNA or anti-miRNA specifically into cancer cells *in vivo* without collateral damage to healthy cells remains challenging. We report here the application of RNA nanotechnology for specific and efficient delivery of anti-miR-21 to block the growth of TNBC in orthotopic mouse models. The 15 nm therapeutic RNA nanoparticles contains the 58-nucleotide (nt) phi29 pRNA-3WJ as a core, a 8-nt sequence complementary to the seed region of miR-21, and a 39-nt epidermal growth factor receptor (EGFR) targeting aptamer for internalizing RNA nanoparticles into cancer cells *via* receptor mediated endocytosis. The RNase resistant and thermodynamically stable RNA nanoparticles remained intact after systemic injection into mice and strongly bound to tumors with little or no accumulation in healthy organs 8 h postinjection, and subsequently repressed tumor growth at low doses. The observed specific cancer targeting and tumor regression is a result of several key attributes of RNA nanoparticles: anionic charge which disallows nonspecific passage across negatively charged cell membrane; "active" targeting using RNA aptamers which increases the homing of RNA nanoparticles to cancer cells; nanoscale size and shape which avoids rapid renal clearance and engulfment by lung macrophages and liver Kupffer cells; favorable biodistribution profiles with little accumulation in healthy organs, which minimizes nonspecific side effects; and favorable pharmacokinetic profiles with extended *in vivo* half-life. The results demonstrate the clinical potentials of RNA nanotechnology based platform to deliver miRNA based therapeutics for cancer treatment.

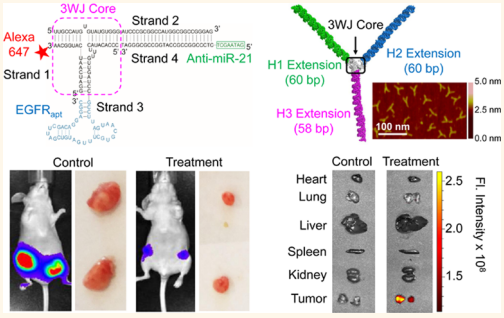

KEYWORDS: RNA nanotechnology · three-way junction · EGFR RNA aptamer · miRNA · triple negative breast cancer

MicroRNAs (miRNAs) are single-stranded noncoding RNAs, typically 19−25 nucleotides that can regulate gene expression at the post-transcriptional level by either degrading their target mRNAs or inhibiting their translation.[1,2] MiRNAs play important roles in regulating cell cycle, proliferation, differentiation, metabolism, and apoptosis.[1] Over the past decade, dysregulation of miRNAs has been implicated in tumor initiation, progression, and metastasis in several cancer types.[3−8] MiRNAs hold great potentials for cancer therapy particularly because one miRNA can regulate a broad set of target genes efficiently and simultaneously, and can therefore address the heterogeneous nature of cancer. Naturally occurring miRNA further displays reduced immune response and low toxicity. Both anti-miRNAs to knockdown oncogenic miRNAs and mimics of miRNAs to upregulate endogenous miRNAs have been developed as therapeutic strategies to achieve tumor regression.[6,9,10] However, the major limiting factor is the ability to specifically deliver these therapeutic modules to affected cells and tissues. Nanotechnology holds great promise in this regard and several nanoplatforms have been pursued, but effective strategies to inhibit tumor progression are still lacking.[11] Major challenges from formulation and delivery perspective include particle heterogeneity, particle aggregation, particle dissociation, unfavorable pharmacokinetics (PK) and pharmacodynamics (PD) profiles, undesirable toxicity and immunogenicity, and difficulties penetrating the tumor

* Address correspondence to dan.shu@uky.edu, peixuan.guo@uky.edu.

Received for review April 24, 2015 and accepted September 5, 2015.

Published online September 05, 2015
10.1021/acsnano.5b02471

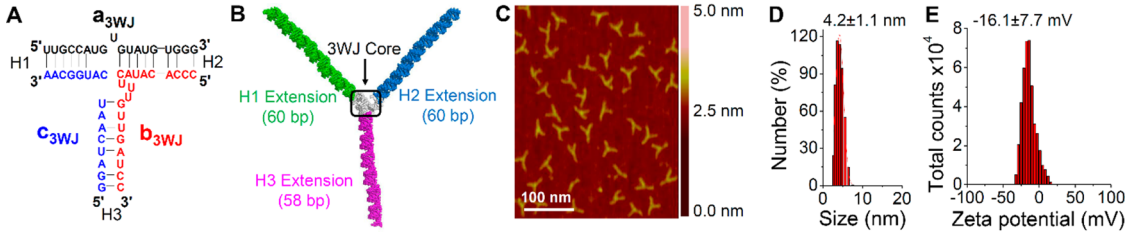

Figure 1. Characterization and introduction of the system for pRNA-3WJ nanoparticle construction. (A) Sequence of phi29 pRNA-3WJ core. (B) 3D model of arm-extended RNA nanoparticles using 3WJ as scaffold. (C) Atomic force microscopy (AFM) image of the nanoparticle in Figure 1B. (D) Size of the 3WJ core determined by dynamic light scattering (DLS). (E) Zeta potential of the 3WJ core.

microenvironment.[11,12] In addition, unstable thermodynamic properties and lack of controlled release mechanisms have slowed their clinical translation.[13] Controlled "active" targeting is desirable to effectively block cancer progression and prevent metastases, while minimizing adverse side effects.[13] Liver and other organ accumulations lead to low cancer targeting and high side-effect or toxicity. Herein, we adopted an RNA nanotechnology approach[14] to overcome some of the aforementioned challenges in cancer nanotechnology and deliver anti-miRNAs to inhibit tumor growth, using triple negative breast cancer (TNBC) as a model system. To date, there are no targeted therapies available for TNBC, an aggressive breast cancer subtype defined by the lack of estrogen receptor, progesterone receptor, and human epidermal growth factor receptor 2 expression.[15] TNBC patients are poorly responsive to chemotherapy, and are susceptible to relapse and early metastatic spread, which leads to poor prognosis and short survival.[16]

RNA nanotechnology, a concept first proved in 1998,[17] refers to the design, fabrication, and application of nanometer scale RNA architectures constructed *via* bottom-up self-assembly with its major frame composed mainly of RNA.[14,17−29] This is distinct from conventional nanomaterials typically used to deliver anti-miRNAs,[30] such as lipid,[31−33] polymer,[34,35] and inorganic nanomaterials.[36] For RNA nanotechnology based particles, scaffolds, targeting ligands, therapeutic moieties, and regulators can all be composed of RNA nucleotides. Another important distinction is that RNA nanotechnology focuses on inter-RNA interactions (between molecules) and quaternary (4D) structure, while classical studies on RNA structure and function focuses on intra-RNA interactions (within a molecule) and secondary (2D)/tertiary (3D) structure. Over the years, several challenges have deterred widespread use of RNA as a construction material, such as sensitivity to RNase degradation; susceptibility to dissociation after systemic injection; and toxicity and adverse immune responses. These three challenges have been overcome to a large extent: 2′-fluoro (2′-F) or 2′-O-methyl (2′-OMe) modifications on the −OH group of the ribose can make the RNA chemically stable in the serum;[37] certain naturally occurring junction motifs are thermodynamically stable and can keep the entire RNA nanoparticle intact at ultralow concentrations;[38−40] and finally, immunogenicity of RNA nanoparticle is sequence and shape dependent, and is tunable to make RNA nanoparticles stimulate the production of inflammatory cytokines,[41] or to make the RNA nanoparticles nonimmunogenic and nontoxic even at repeated i.v. administrations of 30 mg/kg.[42] It is also expected that RNA nanotechnology will play a critical role in the application of exosome RNA for therapy.[43−47]

Herein, we constructed multifunctional RNA nanoparticles using the three-way junction (3WJ) motif (Figure 1)[38,39,48,49] derived from bacteriophage phi29 packaging RNA (pRNA)[50] as a scaffold harboring (1) RNA aptamers as targeting ligands; (2) therapeutic anti-miRNAs; and (3) fluorescent imaging module, Alexa647. To precisely guide and internalize the therapeutic anti-miRNAs to TNBC cells, we used epidermal growth factor receptor (EGFR) targeting RNA aptamers.[51] EGFR is highly amplified (>97%) in both primary TNBC tumors and metastatic TNBC cells.[52,53] As the therapeutic target, we focused on oncogenic miR-21, which is maintained throughout tumor initiation, progression, invasion, and metastasis in varieties of solid cancers, including TNBC.[54−58] We established orthotopic TNBC tumors in nude mice and then systemically administered our multifunctional RNA nanoparticles to determine their targeting and therapeutic effects.

RESULTS

Construction and Characterization of Triple-Functional pRNA-3WJ Nanoparticles. The pRNA-3WJ nanoparticles utilize a modular design composed of three short fragments (Figure 1A).[38] Upon mixing the individual strands in equal molar ratio in PBS or TMS buffer, the complex assembles with high efficiency, as shown in our previous publications.[38,39,48,59] Each branch of the pRNA-3WJ can harbor a functional module without interfering with the folding of the core scaffold and the function of each module, as demonstrated by atomic force microscopy (AFM) images showing homogeneous triangular branched architectures (Figure 1B,C). Herein, we used the pRNA-3WJ core as a scaffold and constructed

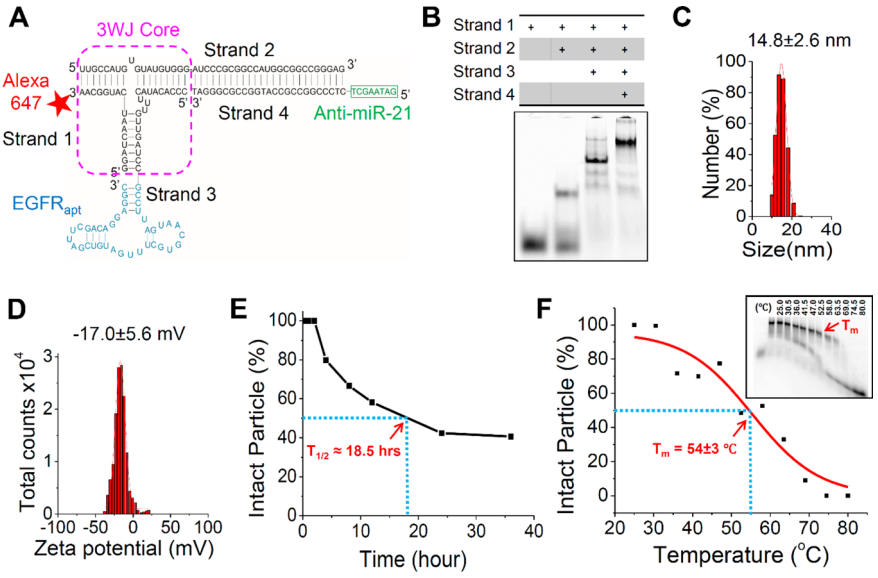

Figure 2. Design and physicochemical characterization of 3WJ-EGFRapt/anti-miR-21 nanoparticles. (A) 2D sequence of the nanoparticle harboring three functional modules: EGFR RNA aptamer for targeted delivery, anti-miR-21 LNA for therapy, and Alexa-647 dye for imaging. (B) Native PAGE showing stepwise highly efficient assembly of the RNA nanoparticle. (C) DLS measurements showing the hydrodynamic size. (D) Zeta potential. (E) Serum stability assay. (F) Apparent T_m extracted from temperature gradient gel electrophoresis (TGGE, insert).

trifunctional RNA nanoparticles 3WJ-EGFRapt/anti-miR-21, harboring EGFR targeting RNA aptamer, therapeutic anti-miR-21 and Alexa-647 as imaging module (Figure 2A). When the four strands were mixed in stoichiometric ratio, the RNA nanoparticle assembled with very high efficiency as indicated by gel shift assays showing stepwise assembly of the complex (Figure 2B).

Dynamic light scattering (DLS) assays showed that the average hydrodynamic diameter of 3WJ-EGFRapt/anti-miR-21 nanoparticles was 14.8 ± 2.6 nm (Figure 2C) compared to 4.2 ± 1.1 nm for pRNA-3WJ core scaffold (Figure 1D). We note that the 3WJ-EGFRapt/anti-miR-21 nanoparticle is not globular in shape, and deviations from DLS measurements are expected, since the reported DLS size corresponds to the average of the three dimensions due to rapid tumbling of RNA nanoparticles in solution.

The particle surface charge, zeta potential, was determined to evaluate the aggregation propensity of RNA nanoparticles in solution. RNA nanoparticles are indeed highly negatively charged and do not aggregate in solution, and this is reflected in the zeta potential measurements showing a single peak at −16.1 ± 7.7 mV for pRNA-3WJ core scaffold (Figure 1E) and −17.0 ± 5.6 mV for 3WJ-EGFRapt/anti-miR-21 nanoparticles (Figure 2D). This aggregation-free physical property and anionic nature is particularly attractive for *in vivo* delivery applications, since it minimizes nonspecific cell entry, and entrapment by lung macrophages and liver Kupffer cells.[11]

To make the 3WJ-EGFRapt/anti-miR-21 nanoparticle chemically stable *in vivo*, we used 2′-F modified U and C nucleotides.[60,61] The 2′-F modified RNA nanoparticles were incubated with 50% fetal bovine serum (FBS) at 37 °C. At defined time points, samples were collected and assayed using native PAGE gel (Figure 2E). The fraction of intact RNA nanoparticles was quantified using ImageJ software and plotted to determine a half-life of about 18.5 h, which is significantly higher than the half-life of unmodified RNA counterparts.[38,60] The presence of 2′-F nucleotides not only makes the RNA nanoparticles resistant to RNase degradation, but also enhances the melting temperature of pRNA-3WJ,[40] without compromising the authentic folding and functionalities of the core and incorporated modules.[37,38]

The 2′-F modified 3WJ-EGFRapt/anti-miR-21 nanoparticles were subjected to temperature gradient gel electrophoresis (TGGE) assay, typically used to determine one of the thermodynamic parameters, the apparent melting temperature (T_m), of RNA nanoparticles composed of multiple strands.[41,48,62,63] One of the strands was labeled with Alexa-647, which was used to determine the fraction of intact particles remaining with increasing temperature gradient (from 25 °C → 80 °C) applied perpendicular to the electric current (Figure 2F, boxed). The fraction of RNA assembled was quantified using ImageJ software and the melting curve was fitted with nonlinear sigmoidal fitting to determine an apparent T_m of 54 ± 3 °C (Figure 2F). The results indicate that the constructed RNA nanoparticle with all the functional modules are thermostable and will remain structurally intact at ultralow concentrations in the body.

Binding and Internalization of pRNA-3WJ Nanoparticles into TNBC Cells. Alexa647 labeled 3WJ-EGFRapt/anti-miR-21 nanoparticles were incubated with MDA-MB-231 cells. The cells were then fixed with paraformaldehyde, and

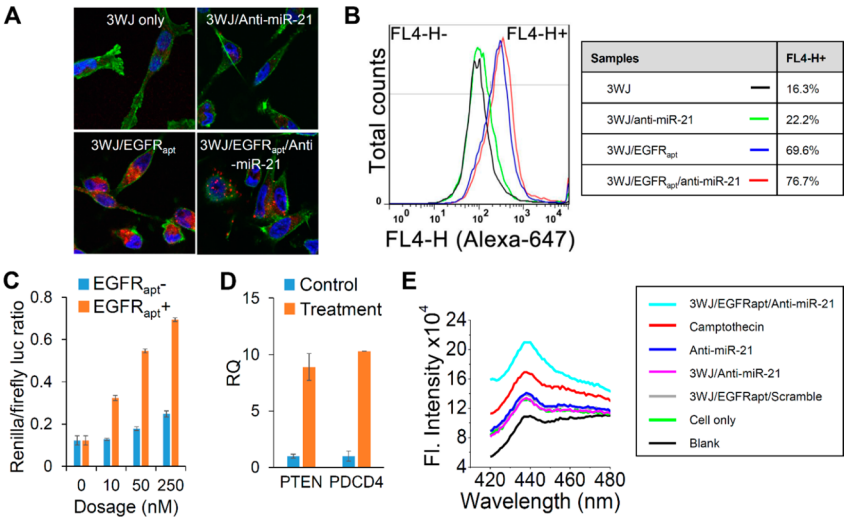

Figure 3. Evaluation of targeting and therapeutic effects of 3WJ-EGFRapt/anti-miR-21 nanoparticles *in vitro*. (A) Confocal images showing efficient binding and internalization into MDA-MB-231 cells. Green: cytoplasm; blue: nuclei; and red: RNA nanoparticles. (B) Flow cytometry assay showing the binding to MDA-MB-231 cells. (C) Dual-luciferase assay demonstrating *in vitro* delivery of anti-miR-21 LNA into MDA-MB-231 cells. (D) qRT-PCR assay depicting the effect of miR-21 knockdown on target gene expression level of PTEN and PDCD4 after treatment. RQ: relative quantification. (E) Caspase-3 assay showing the cellular apoptotic effects of MDA-MB-231 cells after treatment.

the nuclei and cytoplasm were stained using DAPI and Alexa488-phalloidin, respectively. Confocal microscopy images showed very efficient binding and internalization of pRNA-3WJ nanoparticles into cancer cells through EGFR mediated endocytosis, as demonstrated by excellent overlap of fluorescent RNA nanoparticles (red color in Figure 3A) and cytoplasm (green color in Figure 3A). Very low signal was observed for control groups (3WJ scaffold only and 3WJ-anti-miR-21 without EGFR RNA aptamer). The results were further validated using Fluorescence-Activated Cell Sorting (FACS) assay (Figure 3B). The 3WJ-EGFRapt/anti-miR-21 nanoparticles (and controls) were incubated with MDA-MB-231 cells, washed and then analyzed by FACS. Strong binding (76.7%) was observed for EGFR RNA aptamer bearing RNA nanoparticles compared to pRNA-3WJ scaffold control (16.3% binding) (Figure 3B). The results indicate that these RNA nanoparticles have high specificity and affinity for TNBC cell binding.

Delivery of Anti-miR-21 to TNBC Cells by pRNA-3WJ Nanoparticles. We next tested the specific knockdown of oncogenic miR-21 in MDA-MB-231 cells, known to express high levels of miR-21.[57] As anti-miR-21 agent, we used 8-mer (5′-GATAAGCT-3′) locked nucleic acid (LNA, conformationally restricted nucleotide analogues) that is complementary to the miR-21 seed region.[64] LNAs have been reported to bind to their complementary miRNAs with very high affinity and specificity, and are also resistant to exo/endonucleases.[61,65] Upon binding to the miRNA seed region, LNAs will trigger miRNA inhibition in a dose dependent manner.[64]

For assaying miR-21 inhibition, we developed a very sensitive luciferase-based miR-21 reporter system. MDA-MB-231 cells were transfected with a reporter plasmid which contains a miR-21 targeting sequences at the 3′-untranslated regions (UTR) of Renilla Luciferase gene and a coexpressed Firefly Luciferase gene as the internal control. In native cells, the Renilla expression would be repressed, as the miR-21 bind to its 3′-UTR region and prevent the translation of Renilla Luciferase. As anti-miRNA LNA are delivered into the cancer cells, the LNA sequence will competitively bind to miR-21 that used to bind to 3′-UTR region of Renilla Luciferase gene and block its translation, thus resulting in an increased expression of Renilla Luciferase. The results demonstrated that 3WJ-EGFRapt/anti-miR-21 effectively delivered anti-miR-21 LNA sequence into MDA-MB-231 cells after incubation, as indicated by increased Renilla Luciferase expression in a dose dependent manner compared to the control 3WJ-anti-miR-21 nanoparticle without EGFR aptamer (Figure 3C). The successful delivery *via* incubation with cancer cells is a significant advancement in RNAi-based cancer therapeutics, since RNA therapeutics are typically delivered by transfection or microporation methods.

The functionality of miR-21 was validated on its downstream target tumor suppressors, PTEN and PDCD4 genes.[55−57] After incubation with MDA-MB-231 cells, 3WJ-EGFRapt/anti-miR-21 nanoparticles up-regulated the expression of both PTEN and PDCD4, assayed by qRT-PCR at the mRNA levels compared to control 3WJ-anti-miR-21 without EGFR aptamer (Figure 3D).

Effects of pRNA-3WJ Nanoparticles on Growth and Apoptosis of TNBC Cells. Caspase-3 (cysteinyl aspartate-specific protease-3) is an early cellular apoptotic marker, and its activation can be used to assess whether cells are undergoing apoptosis. We found that 3WJ-EGFRapt/anti-miR-21 treated MDA-MB-231 cell lysates showed the highest fluorescence emission of caspase-3 fluorogenic substrate (Ac-DEVD-AMC) comparable to the

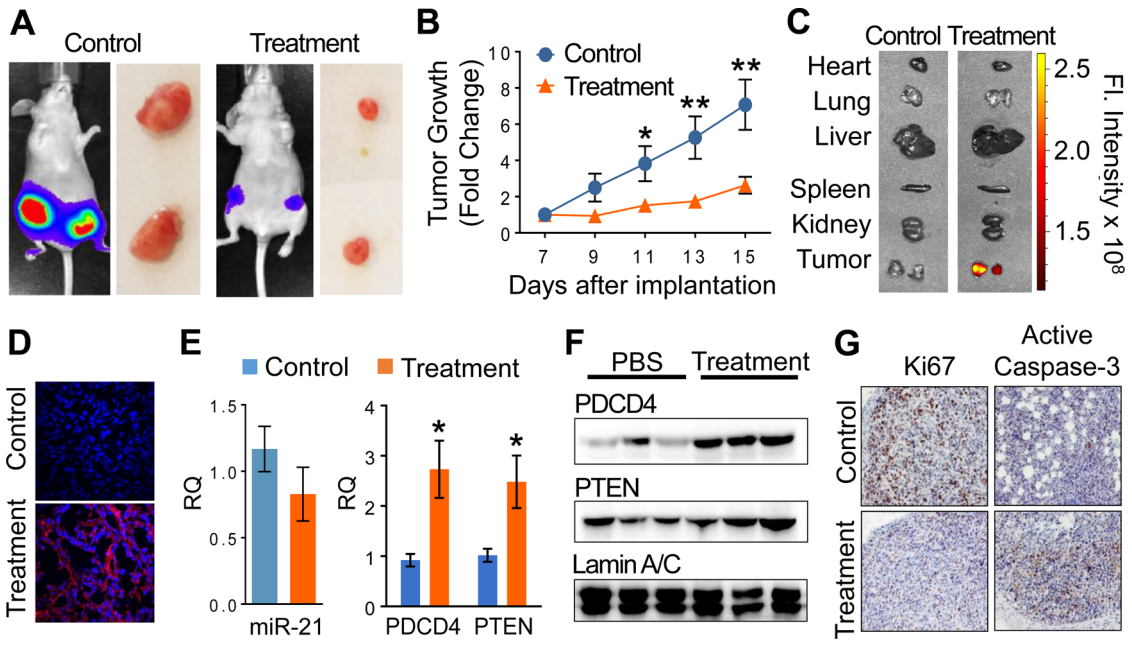

Figure 4. Evaluation of targeting and therapeutic effects of 3WJ-EGFRapt/anti-miR-21 nanoparticles using orthotopic TNBC mouse model. (A) Tumor inhibition over the course of 5 injections. The end point luminescence indicates the tumor volume. (B) Tumor growth curve over the course of 5 injections. (*$P < 0.05$, **$P < 0.01$, error bars indicate SEM). (C) Fluorescence images showing specific targeting and retention in TNBC tumors 8 h postinjection. (D) Histological assay of breast tumor frozen cross sections (10 μm thick) by fluorescence confocal microscopy showing binding and internalization. Blue: nuclei; red: RNA nanoparticle. (E) Real-time PCR at the mRNA level and (F) Western blot at the protein level showing the down-regulation of miR-21 after treatment, resulting in up-regulation of two target genes PTEN and PDCD4. Lamin A/C was internal control. RQ: relative quantification. (G) Immunohistochemistry assay showing inhibition of tumor cell growth after treatment, using Ki67 as indicator of tumor cell proliferation, and active caspase-3 as indicator of tumor cell apoptosis.

positive control camptothecin (CPT), and in contrast to the control RNAs (anti-miR21, 3WJ-anti-miR21, and 3WJ-EGFRapt/Scramble). The results indicate that 3WJ-EGFRapt/anti-miR-21 nanoparticles can activate caspase-3 pathway and trigger cancer cell apoptosis (Figure 3E).

Specific Targeting of TNBC Tumors in Animal Models Assessed by Fluorescence Imaging of RNA Nanoparticles. To evaluate tumor targeting, 3WJ-EGFRapt/anti-miR-21 nanoparticles were systemically administered *via* the tail vein into orthotopic TNBC tumor bearing mice. *Ex vivo* images of normal tissues, organs, and tumors taken after 8 h showed that RNA nanoparticles specifically targeted and accumulated in the tumors, and little or no accumulation was observed in healthy organs and tissues (Figure 4C). In terms of tumor accumulation kinetics, RNA nanoparticles reached their highest accumulation 8 h postinjection and remained in the tumor thereafter for an extended period of time to trigger miRNA knockdown. Such distinct tumor retention behavior is due to the nanoscale size and shape of RNA nanoparticles that are favorable for enhanced permeability and retention (EPR) effects. Histological profiles of breast tumor sections revealed that "active" targeting 3WJ-EGFRapt/anti-miR21 nanoparticles (mediated by EGFR targeting RNA aptamers) strongly bound and internalized into cancer cells, as shown by strong association of RNA nanoparticles (red) with counterstained TNBC cells (Figure 4D).

RNA Nanoparticles for *In Vivo* Targeted Delivery of Anti-miRNA to TNBC Cells. We generated orthotopic TNBC tumors in nude mice using MDA-MB-231 cells expressing luciferase. Upon systemic injection of luciferin, we could visualize the cancer cells using bioluminescence imaging to measure the tumor size and quantitatively assess whether the systemically delivered 3WJ-EGFRapt/anti-miR-21 nanoparticles can down-regulate miR-21 and in the process inhibit tumor growth. TNBC tumor-bearing mice were injected with 3WJ-EGFRapt/anti-miR-21 nanoparticles for 5 times every other day, and the luminescence signal was measured to assess luciferase activity. The end point luminescence signal after 5 doses from the mice treated with 3WJ-EGFRapt/anti-miR-21 RNA nanoparticle were significantly lower than the control treated mice (Figure 4A). This was also evident in the tumor growth curve showing sustained inhibition of tumor growth by 3WJ-EGFRapt/anti-miR-21 nanoparticles compared to the vehicle control (Figure 4B).

To validate anti-miR-21 knockdown at the molecular level, tumor tissues were extracted and lysed. The miR-21 as well as its downstream target mRNAs of PTEN and PDCD4 were quantified by qRT-PCR assay at the mRNA level, and the expression of PTEN and PDCD4 was also examined by Western blot assay at the protein level. The data showed that 3WJ-EGFRapt/anti-miR-21 nanoparticles treated tumors have

reduced miR-21 levels compared to control group (Figure 4E, left panel). The knockdown of miR-21 correlated with increased expression of both PTEN and PDCD4 at both mRNA (Figure 4E, right panel) and protein levels (Figure 4F) for the treatment group compared to the control group. Furthermore, 3WJ-EGFRapt/anti-miR-21 RNA nanoparticle treatment reduced cell proliferation in the tumor tissue, as revealed by decreased Ki67 staining (Figure 4G, left panel), and induced cancer cell apoptosis, as indicated by increased active caspase-3 levels (Figure 4G, right panel), compared to the control group.

DISCUSSION

Since the discovery of RNAi as a key post-transcriptional gene regulation mechanism,[66] it has been proposed for a long time as a potential cancer treatment strategy.[67−73] However, due to the lack of a safe and efficient delivery system, the therapeutic small RNAs including siRNA, miRNA, anti-miRNA and splice-switching oligonucelotides behave poorly *in vivo*. Because of their small size (hydrodynamic diameters typically <5 nm), these small therapeutic RNAs display very short half-life to efficiently trigger their target knockdown[42,74] as they are rapidly cleared by the kidneys.[75] This shortcoming has significantly hindered the clinical translation of RNAi based reagents for disease treatment. Therefore, an effective RNAi delivery system, which can increase the size of the small RNAs as well as introduce cancer specific targeting moieties using cancer cell binding ligands will significantly enhance the pharmacokinetic and therapeutic efficacies of these small therapeutic RNAs.

Here we report for the first time the construction of RNA nanoparticles using the pRNA-3WJ core for specific targeting and delivery of anti-miRNA to cancer cells *in vivo*. Our data indicated that upon systemic injection in orthotopic TNBC tumor bearing mice, 3WJ-EGFRapt/anti-miR-21 nanoparticles can navigate across heterogeneous biological barriers surrounding the tumors to specifically bind and internalize into TNBC cells, knockdown miR-21 resulting in upregulation of PTEN and PDCD4, and efficiently inhibit tumor growth. Moreover, biodistribution studies *in vivo* showed that the RNA nanoparticles can specifically target tumors with little or no accumulation in healthy organs and tissues, which is a significant accomplishment in cancer therapeutics. Specific cancer targeting is a direct result of our RNA nanoparticles physiochemical properties, such as homogeneous size and structure; highly negative charge, which minimizes aggregation propensity and nonspecific entry across negatively charged cell membrane; multivalency to enable combined therapy, targeting and detection, all in one platform; targeted delivery into cancer cells *via* receptor mediated endocytosis using RNA aptamers; advantageous size for favorable biodistribution profiles; a longer *in vivo* terminal half-life (5−12 h) compared to the shorter half-life of bare anti-miRNA and siRNA; and nontoxic and can be manipulated to nonimmunogenic nature.[42] RNA nanoparticles are chemical drugs rather than biological entities, which will facilitate FDA approval process. Taken together, our data demonstrated that pRNA-3WJ nanoparticles have the potential to be applied for clinical applications as a targeted therapeutic delivery system to treat cancer *in vivo*. Because of the ease and flexibility of modification on each RNA module, in the future, different drugs, siRNAs, miRNAs or anti-miRNAs can be incorporated into the RNA nanoparticles as therapeutic functionalities for the treatment of different diseases.

METHODS AND EXPERIMENTAL

Design and Construction of 2′-F Modified pRNA-3WJ Nanoparticles. Multifunctional pRNA-3WJ nanoparticles were constructed using a bottom-up self-assembly approach.[38] The 3WJ-EGFRapt/anti-miR-21 consisted of four fragments (Figure 2A) harboring EGFR targeting RNA aptamer (EGFRapt) as a targeting ligand; AlexaFluor 647 (Invitrogen), as a fluorescent imaging module; and anti-miRNA-21 LNA (anti-miR-21) (Exiqon), as a therapeutic module. The controls include RNA nanoparticles without targeting ligand (denoted as 3WJ-anti-miR-21), without therapeutic module (denoted as 3WJ-EGFRapt), or without therapeutic and targeting modules (denoted as 3WJ).

The core sequences of pRNA-3WJ are as follows[38] (Figure 1A):

a_{3WJ}: 5′-UUG CCA UGU GUA UGU GGG-3′;

b_{3WJ}: 5′-CCC ACA UAC UUU GUU GAU CC-3′;

c_{3WJ}: 5′-GGA UCA AUC AUG GCA A-3′.

The therapeutic 3WJ-EGFRapt/anti-miR-21 is composed of four strands (Figure 2A). Lowercase letters indicate 2′-F modified nucleotides:

Strand 1: 5′-GGA ucA Auc AuG GcA A (C6-NH) (Alexa 647)-3′;

Strand 2: 5′-uuG ccA uGu GuA uGu GGG Auc ccG cGG ccA uGG cGG ccG GGA G-3′;

Strand 3: 5′-ccc AcA uAc uuu Guu GAu ccG ccu uAG uAA cGu Gcu uuG AuG ucG Auu cGA cAG GAG Gc-3′ (underlined sequence is EGFR aptamer[51]);

Strand 4: 5′-+G+A+T+A+A+G+C+T CTC CCG GCC GCC ATG GCC GCG GGA T-3′ (underlined sequence is 8-mer anti-miR21 LNA).

The RNA fragments were synthesized chemically (Trilink and Exiqon) and strands 1−3 are 2′-F modified at cytosine (C) and uracil (U) nucleotides to make the RNA nanoparticles resistant to RNase degradation. The pRNA-3WJ nanoparticles were assembled by mixing the four strands at equal molar concentrations in annealing buffer (10 mM Tris, pH 7.5−8.0, 50 mM NaCl, 1 mM EDTA), and heated to 95 °C for 5 min and slowly cooled to 4 °C over 45 min. Step-wise assembly of the RNA nanoparticles was verified on a native 10% PAGE running in 1× TBE (89 mM Tris-borate, 2 mM EDTA) buffer and imaged by Typhoon FLA 7000 (GE Healthcare) under Cy5 channel.

Characterization of the Assembled pRNA-3WJ Nanoparticle. The assembly of the functionalized 3WJ nanoparticles was characterized by native poly acrylamide gel electrophoresis (PAGE) assays followed by imaging by Typhoon FLA 7000 (GE Healthcare). The structures of the assembled 3WJ complexes were assessed by atomic force microscopy (AFM), and dynamic light scattering

(DLS) as described previously.[38,76−78] RNA images (Figure 1C) were generated using specially modified mica surfaces (APS mica)[77] and imaged with a Veeco MultiMode AFM NanoScope IV system, operating in tapping mode. DLS measurement revealed that the size of the 3WJ core (Figure 1A) was 4.2 ± 1.1 nm (Figure 1D), and the size of the 3WJ-EGFRapt/ant-miR-21 nanoparticle (Figure 2A) was 14.8 ± 2.6 nm (Figure 2C). Because of the resolution limit of AFM image affected by the tip size of 4−10 nm, the size of 3WJ core and 3WJ-EGFRapt/ant-miR-21 nanoparticle were too small to reveal the detail structure and shape. To evaluate the global structures of the RNA nanoparticles derived from the 3WJ core, of which the crystal structure has been solved,[49] 58−60 bp of dsRNA was extended to the three arms of the 3WJ core (Figure 1B). It is expected that 58−60 bp is within the persistence length (stiffness) of 229 bp,[79] thus the AFM image of the resulting arm-extended RNA nanoparticle (Figure 1C) is expected to provide some information about the global structure of RNA nanoparticles derived from the thermodynamically stable 3WJ. Apparent hydrodynamic sizes and zeta potential of preassembled 3WJ (1.5 μM in DEPC H_2O) and 3WJ-EGFRapt/anti-miR-21 (1.35 μM in TBE buffer) were measured by Zetasizer nano-ZS (Malvern Instrument, LTD) at 25 °C, respectively. The data were obtained from three independent measurements.

Temperature Gradient Gel Electrophoresis (TGGE) Assay. The thermodynamic stability of the 2′-F modified 3WJ-EGFRapt/anti-miR-21 nanoparticles was studied using the TGGE system (Biometra GmbH, Germany). One of the fragments (c_{3WJ}) was 3′-end labeled with Alexa647 prior to the assembly of the complex. The 3WJ-EGFRapt/anti-miR-21 nanoparticles were subjected to a 10% native PAGE (2.5 uL of 1 μM RNA nanoparticles per well) and allowed to run in TBM buffer (89 mM Tris, 200 mM boric acid, and 2.5 mM $MgCl_2$) for 5 min at ambient temperature at constant 100 V. After running the RNA into the gel matrix, the gel was transferred into TGGE apparatus and a linear temperature gradient was set up from 25 to 80 °C perpendicular to the electrical current. The gel was run at 80 V for 90 min, and then imaged by Typhoon FLA 7000 (GE Healthcare). The intact particle fraction within the total RNA was analyzed by *ImageJ*, and the melting curve of the construct was fitted using nonlinear sigmoidal fitting. The apparent T_m of the pRNA-3WJ nanoparticle was determined as the temperature at which 50% of the RNA nanoparticle remained assembled.

Serum Stability Assay. The chemical stability of 3WJ-EGFRapt/anti-miR-21 nanoparticles was studied by incubating the RNA nanoparticle with 50% fetal bovine serum (FBS) at 37 °C at final concentration of 2 μM. 10 μL of samples were collected at each time point (0, 0.5, 1, 2, 4, 8, 12, 24, and 36 h) and were subjected to a 10% native PAGE assay with TBM running buffer. The gel was run at 120 V for 120 min, and then imaged by Typhoon FLA 7000 (GE Healthcare). The fraction of intact nanoparticle within the total RNA was analyzed and quantified by *ImageJ*.

Cell Culture. Human TNBC cell line MDA-MB-231 (American Type Culture Collection, ATCC) and MDA-MB-231-Luc (expressing luciferase reporter gene) were grown and cultured in DME/F-12 (1:1) medium (Thermo Scientific) containing 10% FBS inside a 37 °C incubator with 5% CO_2 and a humidified atmosphere.

***In Vitro* Binding Assay Using Fluorescence-Activated Cell Sorting (FACS).** MDA-MB-231 cells were trypsinized and rinsed with blank DME/F-12 (1:1) medium. 100 nM Alexa647 labeled 3WJ-EGFRapt/anti-miR-21 and the control RNA nanoparticles without EGFR aptamer were each incubated with 2×10^5 MDA-MB-231 cells at 37 °C for 2 h. After washing with PBS (137 mM NaCl, 2.7 mM KCl, 100 mM Na_2HPO_4, 2 mM KH_2PO_4, pH 7.4), the cells were resuspended in PBS buffer. FACS was performed using Flow Cytometer (Becton, Dickinson) (available at the University of Kentucky Markey Cancer Center Flow Cytometry and Cell Sorting core facility) to observe the cell binding efficiency of the RNA nanoparticles. The data were analyzed by FlowJo 7.6.1 software.

***In Vitro* Binding and Internalization Assay Using Confocal Microscopy Imaging.** MDA-MB-231 cells were grown on Lab-TekII 8-well chamber slide (Nunc) in DME/F-12 (1:1) medium overnight. 100 nM concentration of Alexa647 labeled 3WJ-EGFRapt/anti-miR-21 and the control 3WJ, 3WJ-EGFRapt, and 3WJ-anti-miR-21 were each incubated with the cells at 37 °C for 2 h. After washing with PBS, the cells were fixed by 4% paraformaldehyde (PFA) and washed 3 times by PBS. The cytoskeleton of the fixed cells was stained by Alexa488 Phalloidin (Life Technologies) for 30 min at room temperature and then rinsed with PBS for 3 × 10 min. The cells were mounted with Prolong Gold antifade reagent. DAPI (Life Technologies) was used for staining the nucleus. The cells were then assayed for nanoparticles binding and cellular entry by FluoView FV1000-Filter Confocal Microscope System (Olympus) (available at the University of Kentucky Markey Cancer Center imaging core facility).

Dual Luciferase Assay to Analyze Delivery of Anti-miR-21 by pRNA-3WJ Nanoparticles. MDA-MB-231 cells were grown on 24-well plates in DME/F-12 (1:1) medium until they reached 80% confluence. Cells were transfected with 150 ng psi-Check 2 plasmid (Promega) which contains an oncogenic miR-21 binding sequences at the 3′-UTR region of Renilla Luciferase gene using Lipofectamine 2000 (Life Technologies). Four hrs after transfection, the medium was replaced with complete DME/F-12 (1:1) medium and the cells were incubated for another 2 h. Various concentration of 3WJ-EGFRapt/anti-miR-21 and the control RNA 3WJ-anti-miR-21 (0, 10, 50, 250 nM) were then incubated with cells in opti-MEM at 37 °C for 2 h, respectively. After incubation with the RNA, complete DME/F-12 (1:1) medium was added into cells and Duel-luciferase assay (Promega) was used to evaluate the anti-miR-21 effects 24 h post-transfection following manufacturer's instruction. Briefly, cells were washed once with PBS and lysed with passive lysis buffer. The cell culture plates were shaken for 15 min at room temperature. 20 μL of the lysate were added to 50 μL of luciferase assay reagent (LAR II) in 96-well plates and control firefly luciferase activity was measured. Upon addition of 50 μL of Stop & Glo Reagent, measurements of Renilla luciferase activity were then obtained. The Renilla luciferase activity was then normalized with respect to the firefly luciferase activity for determining the relative ratio of Renilla to firefly luciferase activity. At least three independent experiments were performed.

Assay the Effects of RNA Nanoparticles on TNBC Cells in Cell Cultures Using qRT-PCR. MDA-MB-231 cells were incubated with 100 nM of the 3WJ-EGFRapt/anti-miR-21 and control RNA nanoparticles, respectively. After 72 h treatment, cells were collected and target gene up-regulation effects were assessed by qRT-PCR at the mRNA level. Cells were processed for total RNA using Trizol RNA extraction reagent following manufacturer's instruction (Life Technologies).

To assay the miR-21 down-regulation, the TaqMan microRNA Assays were performed according to manufacturer's instruction (Life Technologies). Briefly, 10 ng total RNA was used to perform the reverse transcription using TaqMan MicroRNA Reverse Transcription Kit (Life Technologies). MiR-21 specific RT primers were used. Real-time PCR was performed using Taqman Assay. All reactions were carried out in a final volume of 20 μL using Taqman Universal PCR Master Mix and assayed in triplicates. Primers/probe set for human miR-21, and U6 (endogenous control) were purchased from Life Technologies. PCR was performed on StepOne/StepOnePlus systems (Applied Biosystems). The data was analyzed by the comparative CT Method (ΔΔCT Method).

To assay the downstream target genes (PTEN and PDCD4) of miR-21, TaqMan Gene Expression Assays was performed according to manufacturer's instruction (Life Technologies). Briefly, the first cDNA strand was synthesized from total RNA (1 μg) using SuperScript III First-Strand Synthesis System (Life Technologies) from MDA-MB-231 cells with the various RNA nanoparticles treatment. Real-time PCR was performed using Taqman Assay. All reactions were carried out in a final volume of 20 μL using 2 × Taqman Fast Universal PCR Master Mix and assayed in triplicate. Primers/probe set for human PTEN, PDCD4, and 18S (endogenous control) were purchased from Life Technologies. PCR was performed on StepOne/StepOnePlus systems (Applied Biosystem). The data was analyzed by (ΔΔCT Method).

Apoptosis Studies in Cell Culture. In order to assay the cellular effects after RNA nanoparticle treatment, MDA-MB-231 cells were grown on 24-well plates in DME/F-12 (1:1) medium until

they reached 80% confluence. Cells were then treated with 100 nM 3WJ-EGFRapt/anti-miR-21. The controls include anti-miR-21, 3WJ-anti-miR-21, and 3WJ-EGFRapt/Scramble. Twenty-four hours after incubation with the RNAs, the cellular Caspase-3 activity was measured and compared by Caspase-3 Assay Kit (BD Pharmingen) according to manufacturer's instruction. Briefly, cell lysates ($1-10 \times 10^6$ cells/ml) after induction of apoptosis were prepared using cold cell lysis buffer provided by the kit, and incubated for 30 min on ice. For each sample, 50 μL of cell lysate was added with 5 μL reconstituted Ac-DEVD-AMC in HEPES buffer and incubated at 37 °C for 1 h. The amount of AMC liberated from Ac-DEVD-AMC was measured using an excitation wavelength of 380 nm and an emission wavelength range of 420−460 nm on Fluorolog fluorospectrometer (Horiba Jobin Yvon). Camptothecin (CPT) was used as a positive control, which was added into cell culture medium 4 h prior to the analysis of the caspase-3 activity.

Animal Models. All protocols involving animals are performed under the supervision of the University of Kentucky Institutional Animal Care and Use Committee (IACUC). To generate TNBC orthotropic model, female athymic nu/nu mice, 4−8 weeks old, were purchased from Taconic laboratories. Orthotopic tumor xenografts was established by directly injecting 2×10^6 MDA-MB-231-Luc cells resuspended in PBS into the mammary fat pad of nude mice. When the tumor showed sign of growth, the mice were used for assaying therapeutic effects. When the tumor nodules had reached a volume of 100 mm^3 approximately 15 days postinjection, the mice were used for tumor targeting studies.

Fluorescence Imaging to Detect the Binding of RNA Nanoparticles to Orthotopic TNBC Xenografts *In Vivo*. To investigate the delivery of pRNA-3WJ nanoparticles *in vivo*, a fluorescence imaging study was performed after tail vein injection of 100 μL 20 uM Alexa647 labeled 3WJ-EGFRapt/anti-miR-21 into orthotopic TNBC tumor mice. PBS injected mice were used as fluorescence negative control, The mice were sacrificed at 8 h post injection by inhalation of CO_2 followed by cervical dislocation, and major internal organs including heart, lungs, liver, spleen, kidneys together with tumor from the sacrificed mice were collected and subjected to fluorescence imaging for assessment of biodistribution profile using IVIS Spectrum station (Caliper Life Sciences) with excitation at 640 nm and emission at 680 nm. The tumors were further fixed in 4% PFA with 10% sucrose in PBS overnight at 4 °C and embedded in Tissue-Tek O.C.T. compound (Sakura Finetek USA, Inc.) for frozen sectioning (10 μm thick). The sectioned samples were mounted by ProLong Gold Antifade Reagent with DAPI (Life Technologies) overnight. The fluorescent images were obtained using FluoView FV1000-Filter Confocal Microscope System (Olympus) (available at the University of Kentucky Markey Cancer Center Imaging core facility).

Assay for the Therapeutics Effect of RNA Nanoparticles on Regression of TNBC Cells in Animal Models. When the tumor size reached about 5 mm in diameter, TNBC tumor bearing mice were randomly divided into two groups ($N = 12$ each group). One group was injected with RNA nanoparticle 3WJ-EGFRapt/anti-miR-21 through tail vein over the course of 5 injections (Total RNA nanoparticle dose: 5 mg/kg; LNA dose: 0.26 mg/kg) every other day. PBS treated mice were served as treatment control. The tumor volume was measured and monitored every 2 days. The tumor volume was calculated as (length $\times$ width^2)/2. At the beginning and end of the injections, mice were subjected to bioluminescence whole body imaging to detect the endogenous luciferase expression level. Mice were anesthetized and intraperitoneally injected with 150 mg/kg D-luciferin (Biosynth International, Inc.). Bioluminescence from the anesthetized mice was detected by IVIS Spectrum station (Caliper Life Sciences). The mice were then sacrificed, tumors extracted and weighed followed by biochemical and histological analysis.

To quantify the miR-21 and subsequent target gene expression, the tumor tissues were flash frozen in liquid nitrogen and grounded using a mortar. The grounded tumor tissues were transferred to clean centrifuge tubes. Trizol RNA extraction reagent (Life Technologies) was added to extract the total RNA. Then, the miR-21 and subsequent target gene (PTEN and PDCD4) expression were quantified by qRT-PCR using Taqman Assays (Life Technologies) as described above.

Tumor tissues were also lysed in lysis buffer (2% SDS containing phosphatase and protease inhibitor cocktails) (Calbiochem) to quantify target gene expression at the protein level using Western blot assay. Protein concentration was measured by BCA Protein Assay kit (Pierce). Equal amount of total protein was subjected to SDS-PAGE gel electrophoresis and transferred from gel to membrane. Membranes were blocked by 5% fat-free milk at room temperature for 1 h and incubated overnight in primary antibody (PTEN, Cell Signaling, 1:1000; PDCD4, Cell Signaling, 1:1000; Lamin A/C, Santa Cruz, 1:1000). Protein bands were detected with an ECL system (Pierce) after incubating in the HRP-conjugated secondary antibody for 1 h at room temperature and exposed to film for autoradiography.

The therapeutic effects of RNA nanoparticles were evaluated by histological profiling of Ki67 and active caspase-3 activity in tumor tissues. Control and RNA nanoparticles treated group tumor sections were deparaffined by incubating with xylene (10 min once, for three times), and hydrated from 100% ethanol, 95% ethanol, 85% ethanol and 70% ethanol to PBS solution. Slides were then incubated with 3% H_2O_2 for 20 min to block endogenous peroxidase. At the antigen retrieval step, the slides were steamed in 10 mM citrate sodium buffer (pH 6.0) for 30 min. All slides were blocked by 5% goat serum and Avidin/Biotin Blocking Kit (Vector laboratories). Then slides were incubated with primary antibodies (Ki67, Spring Bioscience, 1:500; Active caspase-3, Millipore, 1:100) at 4 °C overnight, and then the sections were incubated with goat antirabbit IgG conjugated with HRP at room temperature for 60 min. The conjugated antibody was detected by diaminobenzidine (DAB). All slides were counterstained with Hematoxylin and images were taken by Nikon microscope.

Statistical Analysis. Each experiment was repeated at least 3 times with duplication for each samples tested. The results were presented as mean $\pm$ standard deviation, unless otherwise indicated. Statistical differences were evaluated using Student's t test, and $p < 0.05$ was considered significant.

Conflict of Interest: The authors declare the following competing financial interest(s): Peixuan Guo is the cofounder of Biomotor and RNA Nanotechnology Development Corp. Ltd..

Acknowledgment. The work was supported by grants EB019036 from NIH/NIBIB and CA151648 from NIH/NCI to P.G. and a DOD grant BC140428 to D.S. and R.X. Service of Shared Resource Facilities was provided by University of Kentucky Markey Cancer Center (P30CA177558). We thank Luda Shlyakhtenko for AFM imaging at the Nanoimaging Core Facility supported by the NIH SIG program and the UNMC Program of ENRI to Yuri Lyubchenko. The funding to Peixuan Guo's Endowed Chair in Nanobiotechnology position is from the William Fairish Endowment Fund.

REFERENCES AND NOTES

1. Bartel, D. P. MicroRNAs: Genomics, Biogenesis, Mechanism, and Function. *Cell* **2004**, *116*, 281–297.
2. Liang, Z.; Wang, X. J. Rising From Ashes: Non-Coding RNAs Come of Age. *J. Genet. Genomics* **2013**, *40*, 141–142.
3. Calin, G. A.; Croce, C. M. MicroRNA Signatures in Human Cancers. *Nat. Rev. Cancer* **2006**, *6*, 857–866.
4. Di, L. G.; Garofalo, M.; Croce, C. M. MicroRNAs in Cancer. *Annu. Rev. Pathol.: Mech. Dis.* **2014**, *9*, 287–314.
5. Garzon, R.; Calin, G. A.; Croce, C. M. MicroRNAs in Cancer. *Annu. Rev. Med.* **2009**, *60*, 167–179.
6. Croce, C. M. Causes and Consequences of MicroRNA Dysregulation in Cancer. *Nat. Rev. Genet.* **2009**, *10*, 704–714.
7. Iorio, M. V.; Ferracin, M.; Liu, C. G.; Veronese, A.; Spizzo, R.; Sabbioni, S.; Magri, E.; Pedriali, M.; Fabbri, M.; Campiglio, M.; *et al.* MicroRNA Gene Expression Deregulation in Human Breast Cancer. *Cancer Res.* **2005**, *65*, 7065–7070.
8. Croce, C. M.; Calin, G. A. MiRNAs, Cancer, and Stem Cell Division. *Cell* **2005**, *122*, 6–7.

9. Kasinski, A. L.; Slack, F. J. Epigenetics and Genetics. MicroRNAs En Route to the Clinic: Progress in Validating and Targeting MicroRNAs for Cancer Therapy. *Nat. Rev. Cancer* **2011**, *11*, 849–864.
10. Henry, J.; zevedo-Pouly, A.; Schmittgen, T. MicroRNA Replacement Therapy for Cancer. *Pharm. Res.* **2011**, *28*, 3030–3042.
11. Grodzinski, P., Torchilin, V., Eds.; *Advanced Drug Delivery Reviews: Cancer Nanotechnology*; Elsevier: Amsterdam, 2014; Vol. 66.
12. Peer, D.; Karp, J. M.; Hong, S.; Farokhzad, O. C.; Margalit, R.; Langer, R. Nanocarriers As an Emerging Platform for Cancer Therapy. *Nat. Nanotechnol.* **2007**, *2*, 751–760.
13. Grodzinski, P.; Farrell, D. Future Opportunities in Cancer Nanotechnology--NCI Strategic Workshop Report. *Cancer Res.* **2014**, *74*, 1307–1310.
14. Guo, P. The Emerging Field of RNA Nanotechnology. *Nat. Nanotechnol.* **2010**, *5*, 833–842.
15. Foulkes, W. D.; Smith, I. E.; Reis-Filho, J. S. Triple-Negative Breast Cancer. *N. Engl. J. Med.* **2010**, *363*, 1938–1948.
16. Fadare, O.; Tavassoli, F. A. Clinical and Pathologic Aspects of Basal-Like Breast Cancers. *Nat. Clin. Pract. Oncol.* **2008**, *5*, 149–159.
17. Guo, P.; Zhang, C.; Chen, C.; Trottier, M.; Garver, K. Inter-RNA Interaction of Phage Phi29 PRNA to Form a Hexameric Complex for Viral DNA Transportation. *Mol. Cell* **1998**, *2*, 149–155.
18. Shu, Y.; Pi, F.; Sharma, A.; Rajabi, M.; Haque, F.; Shu, D.; Leggas, M.; Evers, B. M.; Guo, P. Stable RNA Nanoparticles As Potential New Generation Drugs for Cancer Therapy. *Adv. Drug Delivery Rev.* **2014**, *66C*, 74–89.
19. Guo, P.; Haque, F.; Hallahan, B.; Reif, R.; Li, H. Uniqueness, Advantages, Challenges, Solutions, and Perspectives in Therapeutics Applying RNA Nanotechnology. *Nucleic Acid Ther.* **2012**, *22*, 226–245.
20. Lee, J. B.; Hong, J.; Bonner, D. K.; Poon, Z.; Hammond, P. T. Self-Assembled RNA Interference Microsponges for Efficient SiRNA Delivery. *Nat. Mater.* **2012**, *11*, 316–322.
21. Shopsowitz, K. E.; Roh, Y. H.; Deng, Z. J.; Morton, S. W.; Hammond, P. T. RNAi-Microsponges Form Through Self-Assembly of the Organic and Inorganic Products of Transcription. *Small* **2014**, *10*, 1623–1633.
22. Afonin, K. A.; Viard, M.; Koyfman, A. Y.; Martins, A. N.; Kasprzak, W. K.; Panigaj, M.; Desai, R.; Santhanam, A.; Grabow, W. W.; Jaeger, L.; *et al.* Multifunctional RNA Nanoparticles. *Nano Lett.* **2014**, *14*, 5662–5671.
23. Afonin, K. A.; Kireeva, M.; Grabow, W. W.; Kashlev, M.; Jaeger, L.; Shapiro, B. A. Co-Transcriptional Assembly of Chemically Modified RNA Nanoparticles Functionalized With SiRNAs. *Nano Lett.* **2012**, *12*, 5192–5195.
24. Afonin, K. A.; Grabow, W. W.; Walker, F. M.; Bindewald, E.; Dobrovolskaia, M. A.; Shapiro, B. A.; Jaeger, L. Design and Self-Assembly of SiRNA-Functionalized RNA Nanoparticles for Use in Automated Nanomedicine. *Nat. Protoc.* **2011**, *6*, 2022–2034.
25. Dibrov, S. M.; McLean, J.; Parsons, J.; Hermann, T. Self-Assembling RNA Square. *Proc. Natl. Acad. Sci. U. S. A.* **2011**, *108*, 6405–6408.
26. Geary, C.; Rothemund, P. W.; Andersen, E. S. A Single-Stranded Architecture for Cotranscriptional Folding of RNA Nanostructures. *Science* **2014**, *345*, 799–804.
27. Han, D.; Park, Y.; Kim, H.; Lee, J. B. Self-Assembly of Free-Standing RNA Membranes. *Nat. Commun.* **2014**, *5*, 4367.
28. Lee, T. J.; Haque, F.; Shu, D.; Yoo, J. Y.; Li, H.; Yokel, R. A.; Horbinski, C.; Kim, T. H.; Kim, S.-H.; Nakano, I.; Kaur, B.; Croce, C. M.; Guo, P. RNA Nanoparticles As a Vector for Targeted SiRNA Delivery into Glioblastoma Mouse Model. *Oncotarget* **2015**, *6*, 14766–14776.
29. Li, H.; Rychahou, P. G.; Cui, Z.; Pi, F.; Evers, B. M.; Shu, D.; Guo, P.; Luo, W. RNA Nanoparticles Derived From Three-Way Junction of Phi29 Motor PRNA Are Resistant to I-125 and Cs-131 Radiation. *Nucleic Acid Ther.* **2015**, *25*, 188–197.
30. Zhang, Y.; Wang, Z.; Gemeinhart, R. A. Progress in MicroRNA Delivery. *J. Controlled Release* **2013**, *172*, 962–974.
31. Griveau, A.; Bejaud, J.; Anthiya, S.; Avril, S.; Autret, D.; Garcion, E. Silencing of MiR-21 by Locked Nucleic Acid-Lipid Nanocapsule Complexes Sensitize Human Glioblastoma Cells to Radiation-Induced Cell Death. *Int. J. Pharm.* **2013**, *454*, 765–774.
32. Takahashi, M.; Yamada, N.; Hatakeyama, H.; Murata, M.; Sato, Y.; Minakawa, N.; Harashima, H.; Matsuda, A. *In vitro* Optimization of 2′-OMe-4′-Thioribonucleoside-Modified Anti-MicroRNA Oligonucleotides and Its Targeting Delivery to Mouse Liver Using a Liposomal Nanoparticle. *Nucleic Acids Res.* **2013**, *41*, 10659–10667.
33. Hatakeyama, H.; Murata, M.; Sato, Y.; Takahashi, M.; Minakawa, N.; Matsuda, A.; Harashima, H. The Systemic Administration of an Anti-MiRNA Oligonucleotide Encapsulated PH-Sensitive Liposome Results in Reduced Level of Hepatic MicroRNA-122 in Mice. *J. Controlled Release* **2013**, *173*, 43.
34. Cheng, C. J.; Saltzman, W. M. Polymer Nanoparticle-Mediated Delivery of MicroRNA Inhibition and Alternative Splicing. *Mol. Pharmaceutics* **2012**, *9*, 1481–1488.
35. Babar, I. A.; Cheng, C. J.; Booth, C. J.; Liang, X.; Weidhaas, J. B.; Saltzman, W. M.; Slack, F. J. Nanoparticle-Based Therapy in an *in vivo* MicroRNA-155 (MiR-155)-Dependent Mouse Model of Lymphoma. *Proc. Natl. Acad. Sci. U. S. A.* **2012**, *109*, E1695–E1704.
36. Kim, J. H.; Yeom, J. H.; Ko, J. J.; Han, M. S.; Lee, K.; Na, S. Y.; Bae, J. Effective Delivery of Anti-MiRNA DNA Oligonucleotides by Functionalized Gold Nanoparticles. *J. Biotechnol.* **2011**, *155*, 287–292.
37. Liu, J.; Guo, S.; Cinier, M.; Shlyakhtenko, L. S.; Shu, Y.; Chen, C.; Shen, G.; Guo, P. Fabrication of Stable and RNase-Resistant RNA Nanoparticles Active in Gearing the Nanomotors for Viral DNA Packaging. *ACS Nano* **2011**, *5*, 237–246.
38. Shu, D.; Shu, Y.; Haque, F.; Abdelmawla, S.; Guo, P. Thermodynamically Stable RNA Three-Way Junctions for Constructing Multifuntional Nanoparticles for Delivery of Therapeutics. *Nat. Nanotechnol.* **2011**, *6*, 658–667.
39. Haque, F.; Shu, D.; Shu, Y.; Shlyakhtenko, L.; Rychahou, P.; Evers, M.; Guo, P. Ultrastable Synergistic Tetravalent RNA Nanoparticles for Targeting to Cancers. *Nano Today* **2012**, *7*, 245–257.
40. Binzel, D. W.; Khisamutdinov, E. F.; Guo, P. Entropy-Driven One-Step Formation of Phi29 PRNA 3WJ From Three RNA Fragments. *Biochemistry* **2014**, *53*, 2221–2231.
41. Khisamutdinov, E.; Li, H.; Jasinski, D.; Chen, J.; Fu, J.; Guo, P. Enhancing Immunomodulation on Innate Immunity by Shape Transition Among RNA Triangle, Square, and Pentagon Nanovehicles. *Nucleic Acids Res.* **2014**, *42*, 9996–10004.
42. Abdelmawla, S.; Guo, S.; Zhang, L.; Pulukuri, S.; Patankar, P.; Conley, P.; Trebley, J.; Guo, P.; Li, Q. X. Pharmacological Characterization of Chemically Synthesized Monomeric PRNA Nanoparticles for Systemic Delivery. *Mol. Ther.* **2011**, *19*, 1312–1322.
43. Hunter, M. P.; Ismail, N.; Zhang, X.; Aguda, B. D.; Lee, E. J.; Yu, L.; Xiao, T.; Schafer, J.; Lee, M. L. T.; Schmittgen, T. D.; *et al.* Detection of MicroRNA Expression in Human Peripheral Blood Microvesicles. *PLoS One* **2008**, *3*, e3694.
44. Srivastava, A.; Filant, J.; Moxley, K. M.; Sood, A.; McMeekin, S.; Ramesh, R. Exosomes: A Role for Naturally Occurring Nanovesicles in Cancer Growth, Diagnosis and Treatment. *Curr. Gene Ther.* **2014**, *15*, 182–192.
45. Zhang, H. G.; Grizzle, W. E. Exosomes: A Novel Pathway of Local and Distant Intercellular Communication That Facilitates the Growth and Metastasis of Neoplastic Lesions. *Am. J. Pathol.* **2014**, *184*, 28–41.
46. Redzic, J. S.; Balaj, L.; van der Vos, K. E.; Breakefield, X. O. Extracellular RNA Mediates and Marks Cancer Progression. *Semin. Cancer Biol.* **2014**, *28*, 14–23.
47. Eldh, M.; Olofsson Bagge, R.; Lasser, C.; Svanvik, J.; Sjostrand, M.; Mattsson, J.; Lindner, P.; Choi, D. S.; Gho, Y.; Lotvall, J. MicroRNA in Exosomes Isolated Directly From the Liver Circulation in Patients With Metastatic Uveal Melanoma. *BMC Cancer* **2014**, *14*, 962.
48. Shu, Y.; Haque, F.; Shu, D.; Li, W.; Zhu, Z.; Kotb, M.; Lyubchenko, Y.; Guo, P. Fabrication of 14 Different RNA

Nanoparticles for Specific Tumor Targeting Without Accumulation in Normal Organs. *RNA* **2013**, *19*, 766–777.
49. Zhang, H.; Endrizzi, J. A.; Shu, Y.; Haque, F.; Sauter, C.; Shlyakhtenko, L. S.; Lyubchenko, Y.; Guo, P.; Chi, Y. I. Crystal Structure of 3WJ Core Revealing Divalent Ion-Promoted Thermostability and Assembly of the Phi29 Hexameric Motor PRNA. *RNA* **2013**, *19*, 1226–1237.
50. Guo, P.; Erickson, S.; Anderson, D. A Small Viral RNA Is Required for *in vitro* Packaging of Bacteriophage Phi29 DNA. *Science* **1987**, *236*, 690–694.
51. Esposito, C. L.; Passaro, D.; Longobardo, I.; Condorelli, G.; Marotta, P.; Affuso, A.; de, F. V; Cerchia, L. A Neutralizing RNA Aptamer Against EGFR Causes Selective Apoptotic Cell Death. *PLoS One* **2011**, *6*, e24071.
52. Hynes, N. E.; Lane, H. A. ERBB Receptors and Cancer: the Complexity of Targeted Inhibitors. *Nat. Rev. Cancer* **2005**, *5*, 341–354.
53. Pantel, K.; Brakenhoff, R. H.; Brandt, B. Detection, Clinical Relevance and Specific Biological Properties of Disseminating Tumour Cells. *Nat. Rev. Cancer* **2008**, *8*, 329–340.
54. Zhu, S.; Si, M. L.; Wu, H.; Mo, Y. Y. MicroRNA-21 Targets the Tumor Suppressor Gene Tropomyosin 1 (TPM1). *J. Biol. Chem.* **2007**, *282*, 14328–14336.
55. Frankel, L. B.; Christoffersen, N. R.; Jacobsen, A.; Lindow, M.; Krogh, A.; Lund, A. H. Programmed Cell Death 4 (PDCD4) Is an Important Functional Target of the MicroRNA MiR-21 in Breast Cancer Cells. *J. Biol. Chem.* **2008**, *283*, 1026–1033.
56. Qi, L.; Bart, J.; Tan, L. P.; Platteel, I.; Sluis, T.; Huitema, S.; Harms, G.; Fu, L.; Hollema, H.; Berg, A. Expression of MiR-21 and Its Targets (PTEN, PDCD4, TM1) in Flat Epithelial Atypia of the Breast in Relation to Ductal Carcinoma *in situ* and Invasive Carcinoma. *BMC Cancer* **2009**, *9*, 163.
57. Zhu, S.; Wu, H.; Wu, F.; Nie, D.; Sheng, S.; Mo, Y. Y. MicroRNA-21 Targets Tumor Suppressor Genes in Invasion and Metastasis. *Cell Res.* **2008**, *18*, 350–359.
58. Si, M. L.; Zhu, S.; Wu, H.; Lu, Z.; Wu, F.; Mo, Y. Y. MiR-21-Mediated Tumor Growth. *Oncogene* **2007**, *26*, 2799–2803.
59. Shu, D.; Zhang, L.; Khisamutdinov, E.; Guo, P. Programmable Folding of Fusion RNA Complex Driven by the 3WJ Motif of Phi29 Motor PRNA. *Nucleic Acids Res.* **2014**, *42*, e10.
60. Behlke, M. A. Chemical Modification of siRNAs for *in vivo* Use. *Oligonucleotides* **2008**, *18*, 305–319.
61. Mathe, C.; Perigaud, C. Recent Approaches in the Synthesis of Conformationally Restricted Nucleoside Analogues. *Eur. J. Org. Chem.* **2008**, *2008*, 1489–1505.
62. Jasinski, D.; Khisamutdinov, E. F.; Lyubchenko, Y. L.; Guo, P. Physicochemically Tunable Poly-Functionalized RNA Square Architecture With Fluorogenic and Ribozymatic Properties. *ACS Nano* **2014**, *8*, 7620–7629.
63. Khisamutdinov, E. F.; Jasinski, D. L.; Guo, P. RNA As a Boiling-Resistant Anionic Polymer Material to Build Robust Structures With Defined Shape and Stoichiometry. *ACS Nano* **2014**, *8*, 4771–4781.
64. Obad, S.; dos Santos, C. O.; Petri, A.; Heidenblad, M.; Broom, O.; Ruse, C.; Fu, C.; Lindow, M.; Stenvang, J.; Straarup, E. M.; *et al.* Silencing of MicroRNA Families by Seed-Targeting Tiny LNAs. *Nat. Genet.* **2011**, *43*, 371–378.
65. Castoldi, M.; Schmidt, S.; Benes, V.; Hentze, M. W.; Muckenthaler, M. U. MiChip: an Array-Based Method for MicroRNA Expression Profiling Using Locked Nucleic Acid Capture Probes. *Nat. Protoc.* **2008**, *3*, 321–329.
66. Fire, A.; Xu, S.; Montgomery, M. K.; Kostas, S. A.; Driver, S. E.; Mello, C. C. Potent and Specific Genetic Interference by Double-Stranded RNA in Caenorhabditis Elegans. *Nature* **1998**, *391*, 806–811.
67. Wu, S. Y.; Lopez-Berestein, G.; Calin, G. A.; Sood, A. K. RNAi Therapies: Drugging the Undruggable. *Sci. Transl. Med.* **2014**, *6*, 240ps7.
68. Tabernero, J.; Shapiro, G. I.; Lorusso, P. M.; Cervantes, A.; Schwartz, G. K.; Weiss, G. J.; Paz-Ares, L.; Cho, D. C.; Infante, J. R.; Alsina, M.; *et al.* First-in-Man Trial of an RNA Interference Therapeutic Targeting VEGF and KSP in Cancer Patients With Liver Involvement. *Cancer Discovery* **2013**, *3*, 406–417.
69. Bora, R. S.; Gupta, D.; Mukkur, T. K.; Saini, K. S. RNA Interference Therapeutics for Cancer: Challenges and Opportunities (Review). *Mol. Med. Rep.* **2012**, *6*, 9–15.
70. Tiemann, K.; Rossi, J. J. RNAi-Based Therapeutics-Current Status, Challenges and Prospects. *EMBO Mol. Med.* **2009**, *1*, 142–151.
71. Aagaard, L.; Rossi, J. J. RNAi Therapeutics: Principles, Prospects and Challenges. *Adv. Drug Delivery Rev.* **2007**, *59*, 75–86.
72. Bumcrot, D.; Manoharan, M.; Koteliansky, V.; Sah, D. W. RNAi Therapeutics: a Potential New Class of Pharmaceutical Drugs. *Nat. Chem. Biol.* **2006**, *2*, 711–719.
73. Robinson, R. RNAi Therapeutics: How Likely, How Soon? *PLoS Biol.* **2004**, *2*, e28.
74. Morrissey, D. V.; Lockridge, J. A.; Shaw, L.; Blanchard, K.; Jensen, K.; Breen, W.; Hartsough, K.; Machemer, L.; Radka, S.; Jadhav, V.; *et al.* Potent and Persistent *in vivo* Anti-HBV Activity of Chemically Modified siRNAs. *Nat. Biotechnol.* **2005**, *23*, 1002–1007.
75. Longmire, M.; Choyke, P. L.; Kobayashi, H. Clearance Properties of Nano-Sized Particles and Molecules As Imaging Agents: Considerations and Caveats. *Nanomedicine (London, U. K.)* **2008**, *3*, 703–717.
76. Lyubchenko, Y. L.; Shlyakhtenko, L. S.; Ando, T. Imaging of Nucleic Acids With Atomic Force Microscopy. *Methods* **2011**, *54*, 274–283.
77. Lyubchenko, Y. L.; Shlyakhtenko, L. S. AFM for Analysis of Structure and Dynamics of DNA and Protein-DNA Complexes. *Methods* **2009**, *47*, 206–213.
78. Lyubchenko, Y. L.; Gall, A. A.; Shlyakhtenko, L. S.; Harrington, R. E.; Jacobs, B. L.; Oden, P. I.; Lindsay, S. M. Atomic Force Microscopy Imaging of Double Stranded DNA and RNA. *J. Biomol. Struct. Dyn.* **1992**, *10*, 589–606.
79. Abels, J. A.; Moreno-Herrero, F.; van der Heijden, T.; Dekker, C. F.; Dekker, N. H. Single-Molecule Measurements of the Persistence Length of Double-Stranded RNA. *Biophys. J.* **2005**, *88*, 2737–2744.